# Turbulence spreading as a non-local mechanism of global confinement degradation and ion temperature profile stiffness

**S. Yi[1], J.M. Kwon[1], P.H. Diamond[2], and T.S. Hahm[1,3]**

[1] National Fusion Research Institute, Daejeon 305-333, Republic of Korea

[2] Center for Astrophysics and Space Sciences and Department of Physics, University of California at San Diego, La Jolla, CA 92093-0424, USA

[3] Department of Nuclear Engineering, Seoul National University, Seoul 151-744, Republic of Korea

E-mail: yism@nfri.re.kr

**Abstract.** A new non-local mechanism of the global confinement degradation and ion temperature profile stiffness is proposed based on the results of global gyrokinetic simulations. We find that turbulence spreading into a marginally stable zone can increase turbulent transport to a level exceeding the predictions of the local theories. Also, we present the first quantification of the parametric dependence of turbulence spreading and resulting confinement degradation on toroidal rotation shear and magnetic shear: turbulence spreading is significant for high magnetic shears $s > 0.2$, while it is slowed for low magnetic shears. The suppression of turbulence spreading by toroidal rotation shear is only effective for the low magnetic shears, which is in a good agreement with the experimental trends of core confinement improvement. Our findings suggest that the non-local mechanism is indispensable for an accurate transport modeling in tokamak plasmas.

PACS numbers: 52.35.Mw, 52.35.Ra,52.55.Fa,52.65.Tt

Submitted to: *Nucl. Fusion*

In tokamak experiments with intensive ion heating, it is commonly observed that ion heat transport becomes turbulent and increases very sharply as ion temperature gradient exceeds the threshold for ion temperature gradient(ITG) instabilities[1, 2, 3]. This so-called profile stiffness phenomenon limits the achievable maximum central ion temperature $T_i(0)$. Therefore, understanding the physical mechanisms of turbulent ion heat transport and $T_i$ profile stiffness is necessary for the enhancement of tokamak performance and the achievement of controlled fusion.

The level of turbulent ion heat transport depends on various experimental parameters. The well-known key parameters are magnetic shear and toroidal rotation shear. Both weak or negative magnetic shear and high toroidal rotation shear facilitate the improvement of core ion thermal confinement[3, 4, 5]. Recent experiments on the JET tokamak clarified that strong turbulent transport appears in the low rotation plasmas, while it is significantly reduced by combined high rotation shear and low magnetic shear[5]. The dependence of the core confinement on these two key parameters is interpreted primarily based on local properties of micro-turbulence such as $E \times B$ decorrelation of local turbulence. However, the local models are insufficient to explain the parametric dependency of the confinement. In particular, results of the local models often underestimate the level of turbulent transport as compared to the experimental results[6, 7, 8, 9]. The underestimation by the local models implies the existence of other mechanisms which increase ion heat transport.

In searching the missing transport mechanisms for the confinement degradation and resulting $T_i$ profile stiffness against external heating, fluctuation measurements during the evolution of internal transport barrier (ITB), which is a prime example of core confinement improvement, provide an important clue. For instance, before the formation of ITB, the radial correlation length of the fluctuation was estimated to be much longer than the typical predictions of the local theories[10]. As the level of turbulent transport decreased with the development of an ITB, the correlation length decreased to the level expected from the local theories [10, 11]. These experimental observations suggest that the core confinement can be improved by the inhibition of turbulence penetration into the ITB region, and that non-local transport mechanisms degrade core confinement and increase the profile stiffness.

In this letter, we propose a new physical picture to understand the non-local character of turbulent ion heat transport and $T_i$ profile stiffness based on turbulence spreading[12, 13, 14, 15, 16, 17]. Turbulence spreading is a prime example of the non-local mechanisms for confinement degradation, since fluctuation energy can be directly transferred to distant regions by nonlinear spectral interactions during the spreading. So, fluctuation from a strongly driven region can raise turbulent transport in a marginally stable or weakly turbulent region, and thus degrades the global confinement.

We explore the dependence of turbulence spreading on magnetic shear and toroidal rotation shear and its impact on ion heat transport. To this end, we perform a set of carefully designed numerical experiments in which turbulence is triggered by an identical

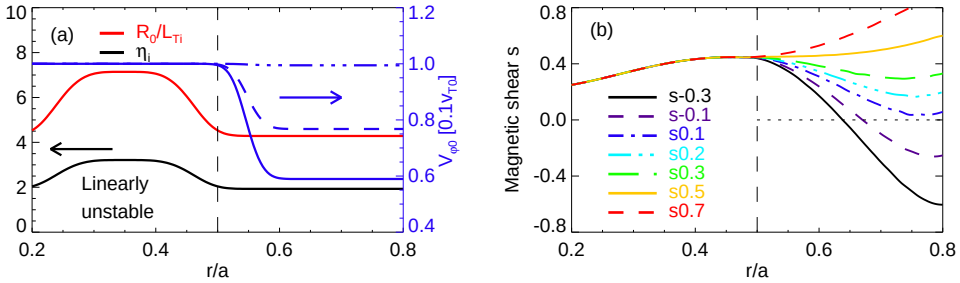


**Figure 1.** (a) Initial profiles of ion temperature gradient, $\eta_i$, and external toroidal rotation $V_{\varphi 0}$ with the various shear of $U_0' = 0, 0.4, 0.8$. (b) Radial profiles of magnetic shear $s$.

linear ITG instability in a source region, and then propagates into marginally stable regions with different toroidal rotation and magnetic shear profiles (This setup ensures that only the turbulence spreading is responsible for heat transport in the stable region). Then, we analyze the responses of fluctuation intensity and heat flux in the stable region. *In this work, we find that turbulence spreading into the marginally stable zone increases turbulent transport to a level exceeding the predictions of local theories. Also, we find that the dependence of the spreading-induced transport on toroidal rotation shear and magnetic shear is the same as the experimental trends[5].*

We use a global $\delta f$ gyrokinetic particle-in-cell code `gKPSP` [18]. The separation of local linear physics and non-local spreading is essential in this study. To facilitate the separation, we use the following simulation setup. The radial domain is divided into two regions, an inner core and the outer region with linearly unstable $R_0/L_{Ti} \equiv R_0(dT_i/dr)/T_i = 7.1$ ($\eta_i \equiv L_n/L_{Ti} = 3.2$) and marginally stable $R_0/L_{Ti} = 4.3$ ($\eta_i = 1.9$) values, respectively. Figure 1(a) shows the initial profiles of $R_0/L_{Ti}$ and $\eta_i$. ITG turbulence is excited in the unstable core region with $0.2 < r/a < 0.5$, and spreads into the stable outer region with $r/a > 0.5$. Here $R_0$ and $a$, respectively, represent the major and minor radius of the torus with the aspect ratio $R_0/a = 3.1$. We consider a medium-size plasma of $\rho_{i0}/a = 1/167$ with a concentric circular equilibrium, where $\rho_{i0}$ is the ion gyroradius in the center.

We employ a set of external toroidal rotation $V_{\varphi 0}$ and magnetic shear $s \equiv (r/q)(dq/dr)$ profiles as shown in Fig.1. The profiles are chosen to provide an identical linear instability in the core, with variations in the stable outer region. The rotation velocity in the center is set to $0.1v_{T0}$, where $v_{T0} = 3.8 \times 10^7$ cm/sec is the ion thermal velocity in the center. The rotation profiles have a range of radial shearing as $U_0' \equiv -(a/v_{T0})(dV_{\varphi 0}/dr) = 0{-}0.8$ in the stable region $r/a = 0.55$ (we note that $U_0' \sim 0.5$ in the JET experiments[5]). For a given $V_{\varphi 0}$ profile, we calculate the neoclassical equilibrium $E_{r0}$ using the radial force balance equation $E_{r0} = (\partial P_i/\partial r)/(en_0) - V_{\theta,neo}B_\varphi + V_{\varphi 0}B_\theta$, and add the calculated $E_{r0}$ to the self-consistently calculated radial electric field in the simulations. Figure 1(b) shows the magnetic shear profiles (numerical values in the labels are magnetic shear at a reference position $r/a = 0.7$ in the stable region). The

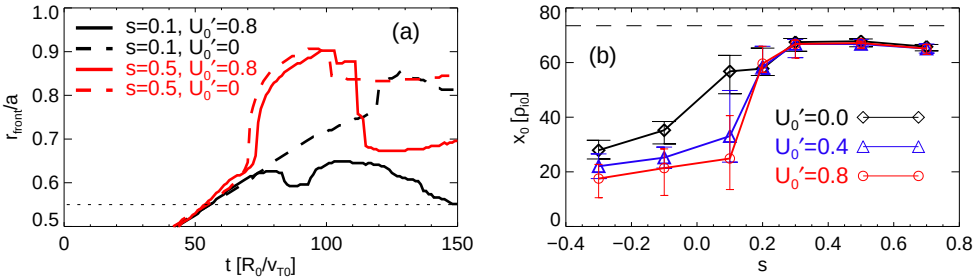


**Figure 2.** (a) Position of the front of turbulence intensity profile in time for different $s$ and $U_0'$. The dotted, horizontal line indicates the location of the rotation shear. (b) Penetration depth $x_0$ as a function of $s$ for different $U_0'$.

variation range of $s$ covers core magnetic shear values in typical tokamak experiments.

We note that there is no profile control during the simulations, so turbulence ultimately decays as free energy in the profile gradients is exhausted. However, turbulence penetration into the linearly stable region is faster than turbulence decay. Quantitatively, the ratio of the penetration time to the decay time is $\gamma_{decay}\Delta t_{spread} = 0.1 - 0.4$. Here we define $\gamma_{decay} \equiv I^{-1}|\partial I/\partial t|$ after local nonlinear saturation in the linearly unstable region, where $I = \langle(e\delta\phi/T_{i0})^2\rangle$ is the intensity of the normalized electrostatic potential fluctuation.

The dynamics of turbulence spreading varies clearly for different values of rotation and magnetic shear. It is well known that external $E\times B$ shearing can hinder turbulence spreading[19]. We find that the suppression of spreading depends strongly on magnetic shear, as well. To be quantitative, we define the turbulence front as the value of turbulence intensity $I \approx 0.05I_0$, where $I_0$ denotes the nonlinear saturation level of the turbulence intensity in the unstable region. Figure 2(a) shows the temporal evolution of the radial position of the front due to spreading. Without rotation shear ($U_0' = 0.0$), the turbulence front propagates promptly up to the simulation boundary at $r > 0.9a$ in the high magnetic shear case $s = 0.5$. On the other hand, in the low magnetic shear case $s = 0.1$, the propagation speed is much slower compared to the high $s$ case, though the penetration depth is similar. The slow propagation speed implies slowing down of turbulence spreading processes, and thus easier control of the spreading by external means (this argument will be substantiated more quantitatively in the later part of this letter). In the presence of a strong rotation shear $U_0' = 0.8$, turbulence spreading persists in the high $s$ case, while the spreading is effectively suppressed in the low $s$ case, as shown by the solid curves in Fig.2(a).

Figure 2(b) shows the dependence of the turbulence penetration depth $x_0$ on $s$ and $U_0'$. The depth is measured as the distance of the turbulence front ($I_{front} \equiv 0.05I_0$) from the boundary of the linearly unstable region at $r/a = 0.5$. The error bars represent the variations of $x_0$ as we define the turbulence front with the different values of turbulence intensity $I_{front} \equiv (0.05 \pm 0.03)I_0$. The horizontal broken line denotes the simulation buffer zone where fluctuations get damped artificially. We can clearly see that turbulence

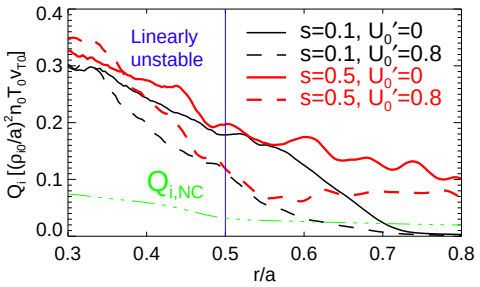


**Figure 3.** Profiles of turbulent heat flux $Q_i$ for different $s$ and $U_0'$. Neoclassical heat transport $Q_{i,NC}$ is denoted by the green line.

spreading is promoted by positive magnetic shear and maximized around $s \sim 0.5$. As the magnetic shear decreases from the optimal range, the penetration becomes weaker i.e. both the penetration depth and speed decrease. The variation of $U_0'$ shows a very interesting trend. The suppression of turbulence spreading is only effective when $s$ is lower than 0.2. The rotation shear is ineffective at high magnetic shear.

From the close relation between turbulence intensity $I$ and turbulent heat flux $Q_i \sim -\chi \partial T_i/\partial r \sim -I\partial T_i/\partial r$, we expect that heat transport in the stable region is proportional to turbulence spreading. Figure 3 shows profiles of the heat flux, which are averaged over a time period during which the spreading is saturated. It is clear from the figure that, when the magnetic shear is high ($s = 0.5$), turbulence spreading causes turbulent transport at radii beyond the unstable region for all the rotation shear values. In the marginally stable region, the turbulent heat transport induced by the spreading dominates the neoclassical transport. This implies that turbulent transport in a marginally stable or weakly turbulent region can be increased by fluctuation from strongly driven regions. Ion heat confinement in experiments can be worse than the predictions of local models.

When spreading is suppressed by toroidal rotation shear at low $s$, turbulent transport is localized in the driving region, as shown by the broken-black line in Fig.3. The rotation shear combined with low $s$ prevents the degradation of local confinement in the stable region by the spreading, implying the preservation of local confinement to the level set by local mechanisms.

To understand the benefits of low or negative magnetic shears for the suppression of turbulence spreading, we examine the dependence of the characteristic time scale of turbulence spreading $\tau_N$ on magnetic shear. If we denote the diffusivity of turbulence spreading as $D$, the time scale of the spreading can be estimated by the mixing rule as $\tau_N = \langle r_c \rangle^2 / D$, where $\langle r_c \rangle$ corresponds to the radial correlation length of turbulence. For the estimation of $\tau_N$, the evaluation of the diffusivity $D$ is essential. By performing a fluctuation intensity transport analysis, we estimate the diffusivity $D$ (the details of the analysis can be found in Ref.[20]).

Figure 4(a) shows the diffusion coefficient $D$ as a function of $s$ for the cases with $U_0' = 0$, where the spreading is not suppressed. The error bars denote the uncertainty

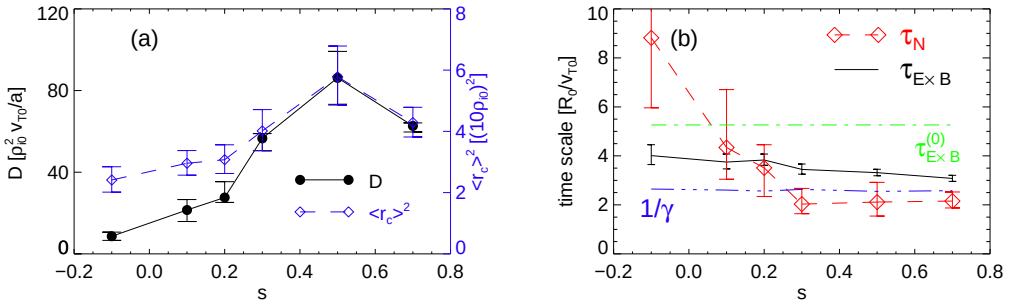


**Figure 4.** (a) Diffusion coefficient $D$ (black) and square of radial correlation length (blue) as a function of $s$ in the cases of $U_0' = 0$. (b) Nonlinear spreading time $\tau_N$ (red) and $E \times B$ decorrelation time $\tau_{E\times B}$ (black) as a function of $s$. $\tau_{E\times B}$ in the cases of $U_0' = 0.8$ is presented.

of the estimated $D$ due to the variations of $x_0$ in Fig. 2(b). The $s$-dependence of the diffusivity is similar to the dependence of the penetration depth. Next, we estimate the radial correlation length of fluctuation as

$$\langle r_c \rangle = \int dV r_c(\theta,\varphi)\phi^2(r,\theta,\varphi) / \int dV \phi^2(r,\theta,\varphi),$$

where $dV = rd\theta Rd\varphi dr$. The average is taken in the low-field side of $|\theta| \leq \pi/8$ for the whole toroidal angle $\varphi$. At each poloidal and toroidal angle, the correlation length $r_c(\theta,\varphi)$ is estimated from the width of the dominant peak in the $k_r$ power spectrum, defined as $r_c = 4/\Delta k_r$. The radial domain of the estimation is chosen in the linearly stable region $r > 0.5a$. The correlation length is averaged over a time period during which the fluctuation front sweeps into the stable region. The square of $\langle r_c \rangle$ is represented by the blue curve in Fig. 4(a). The standard deviation $\sigma$ of the time average is indicated by error bars ($\pm 1\sigma$). Because the decrease of $D$ for decreasing $s$ is more rapid than that of $\langle r_c \rangle^2$, the spreading time $\tau_N$ increases for decreasing $s$, as shown in Fig. 4(b) by the red curve (the error bars represent the variability of $\tau_N$ caused by the variations of $D$ and $\langle r_c \rangle$). The divergent behavior of $\tau_N$ in low magnetic shears ($s < 0.2$) clarifies the observed slowing down of turbulence spreading.

We compare the spreading time $\tau_N$ with the effective $E \times B$ decorrelation time, defined by the inverse of the maximum amplitude of the total $E \times B$ rotation shear, $\tau_{E\times B} \equiv 1/max(|\omega_{E\times B}|)$. The total $E \times B$ shear consists of the externally imposed equilibrium part and the self-generated zonal component, i.e. $\omega_{E\times B} = \omega^{(0)}_{E\times B} + \omega^{(ZF)}_{E\times B}$, where $\omega^{(C)}_{E\times B} = (r/q)\partial(qE^{(C)}_r/rB_\varphi)/\partial r$ for equilibrium ($C = 0$) and zonal part ($C = ZF$)[21]. The decorrelation time $\tau_{E\times B}$ is averaged over a time period over which the suppression of spreading is apparent. This is shown in Fig. 4(b) by the black curve with the error bars of $\pm 1\sigma$. We find that the spreading time $\tau_N$ becomes longer than the decorrelation time $\tau_{E\times B}$ for low magnetic shears ($s < 0.2$). This behavior results in the effective suppression of turbulence spreading by toroidal rotation shear for low $s$. We note that the inverse of the linear growth rate (the blue line) cannot explain the benefit of low magnetic shear in the suppression, because the inverse of the growth rate

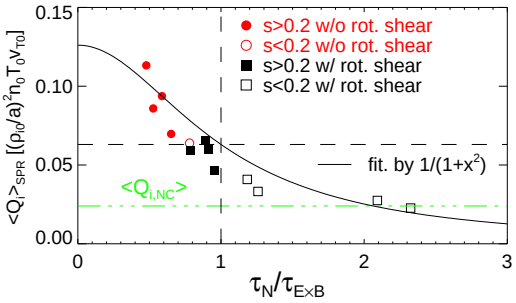


**Figure 5.** Heat flux averaged over the linearly stable region as a function of the ratio of the spreading time to the decorrelation time $\tau_N/\tau_{E\times B}$.

is independent of magnetic shear in the stable region and also smaller than $\tau_{E\times B}$, as shown in Fig.4(b).

The behavior of total $E \times B$ shear also merits some additional discussion. In the presence of equilibrium toroidal rotation shear, zonal flow shear develops in the opposite direction of $\omega^{(0)}_{E\times B}$, but its amplitude dominates that of the equilibrium rotation shear contribution. The resulting total $E \times B$ decorrelation is stronger than that of the equilibrium contribution only, as shown in Fig. 4(b) by the green line. When we apply toroidal rotation shear in the opposite direction ($U_0' < 0$), the amplitude of the total $\omega_{E\times B}$ is similar, but its direction becomes opposite, to the cases with $U_0' > 0$. The rotation shear of $U_0' < 0$ also suppresses turbulence spreading to the levels similar to the $U_0' > 0$ cases. These observations imply that the suppression of turbulence spreading is a self-organized process, which does not result from the direct addition of an external $E \times B$ shearing only. Although interplay between self-generated zonal electric field and equilibrium $E_r$ is an important issue, this is beyond the scope of this work and deferred to a subsequent paper.

The analysis of the time scales suggests that the ratio of the spreading time to the decorrelation time $\tau_N/\tau_{E\times B}$ is a key parameter determining the degradation of local confinement by the spreading and its inhibition. Figure 5 shows the mean turbulent heat flux in the linearly stable region $\langle Q_i \rangle_{SPR}$ as a function of the time scale ratio $\tau_N/\tau_{E\times B}$. Heat flux induced by turbulence spreading rapidly increases with decreasing $\tau_N/\tau_{E\times B}$. The simulation results are in an agreement with the conventional scaling of the $E \times B$ shear quenching $Q_i \sim Q_{i0}/[1 + (\tau_N/\tau_{E\times B})^2]$, as shown by the solid curve in Fig.5. The ratio $\tau_N/\tau_{E\times B}$ varies according to the combination of $s$ and $U_0'$ as follows. The cases without rotation shear show the smallest values of $\tau_N/\tau_{E\times B} < 1.0$. For high $s > 0.2$, the ratio mildly increases to $\tau_N/\tau_{E\times B} \leq 1.0$ as $U_0'$ increases. For low $s < 0.2$, the rotation shear elevates the parameter to $\tau_N/\tau_{E\times B} > 1.0$.

If the level of turbulent transport is quantified by the stiffness factor defined by the increment of heat flux as a function of ion temperature gradient above the threshold[1], the confinement degradation by spreading contributes to the increase of the stiffness factor. We notice that our result is consistent with the finding of the stiffness experiment

on JET[5]: In low $V_{\varphi 0}$ cases, strong profile stiffness appears independent of $s$. In high $V_{\varphi 0}$ cases, the stiffness is significantly reduced by low $s$, while the stiffness reduction is modest for high $s$. The experimental criterion of $s_{c,ex} = 0.35$ separating the low and high magnetic shear, and our finding $s_{c,th} = 0.2$ are within experimental uncertainties and the variations of $s$-profiles in this work. We note that the results of local analyses show much smaller stiffness factors as compared to the observed values of the low rotation discharges[8, 9], while a local result explains the reduced stiffness factor in the high rotation discharges[22]. The discrepancy between the local models and the experimental results can be reconciled by the non-local transport induced by turbulence spreading.

In summary, we elucidated the effect of turbulence spreading, which degrades global ion thermal confinement and increases $T_i$ profile stiffness, and its parametric dependence on toroidal rotation shear and magnetic shear. We found that low or negative magnetic shear slows down turbulence spreading. The inhibition of the spreading by toroidal rotation shear is only effective for the low or negative magnetic shear ($s < 0.2$). Thus, the combined low or negative magnetic shear and high toroidal rotation shear can contribute to $T_i$ profile de-stiffening and the global confinement improvement. For high magnetic shear, on the other hand, turbulence spreading from a strongly driven region can degrade the global confinement. Therefore, we propose that the omission of turbulence spreading and its non-local effects in transport modeling can lead to an underestimation of the level of turbulent transport and inferior understanding of plasma confinement scaling on toroidal rotation and magnetic shear.

The theoretical picture suggested in this letter is testable in profile de-stiffening experiments. We propose to measure the bicoherence of fluctuation spectra in different radii[23, 24]. If turbulence spreading contributes to core confinement degradation, the non-local bicoherence will change as the level of turbulent transport varies.

## Acknowledgments

The authors thank the participants 4th APTWG conference for valuable discussions. This work was supported by R&D Program through National Fusion Research Institute (NFRI) funded by the Ministry of Science, ICT and Future Planning of the Republic of Korea (NFRI-EN1541-1) and by U.S. Department of Energy under Award No. DE-FG02-04ER54738 and CMTFO.

## References

[1] Garbet X. *et al* 2004 *Plasma Phys. Control. Fusion* **46** 1351
[2] Baker D.R. *et al* 2001 *Phys. Plasmas* **8** 4128
[3] Wolf R.C. *et al* 2003 *Plasma Phys. Control. Fusion* **45** 1757
[4] Mantica P. *et al* 2009 *Phys. Rev. Lett.* **102** 175002
[5] Mantica P. *et al* 2011 *Phys. Rev. Lett.* **107** 135004
[6] Holland C. *et al* 2011 *Phys. Plasmas* **18** 056113
[7] Rhodes T.L. *et al* 2011 *Nucl. Fusion* **51** 063022
[8] Mantica P. *et al* 2011 *Plasma Phys. Control. Fusion* **53** 124033

[9] Citrin J. *et al* 2014 *Nucl. Fusion* **54** 023008
[10] Nazikian R. *et al* 2005 *Phys. Rev. Lett.* **94** 135002
[11] Ida K. *et al* 2008 *Phys. Rev. Lett.* **101** 055003
[12] Garbet X., Laurent L., Samain A. and Chinardet J. 1994 *Nucl. Fusion* **34** 963
[13] Diamond P.H. and Hahm T.S. 1995 *Phys. Plasmas* **2** 3640
[14] Hahm T.S., Diamond P.H., Lin Z., Itoh K. and Itoh S.-I. 2004 *Plasma Phys. Control. Fusion* **46** A323
[15] Gürcan Ö.D., Diamond P.H., Hahm T.S. and Lin Z. 2005 *Phys. Plasmas* **12** 032303
[16] Naulin V., Nielsen A. H. and Rasmussen J. J. 2005 *Phys. Plasmas* **12** 122306
[17] Yagi M., Ueda T., Itoh S.-I., Azumi M., Itoh K., Diamond P.H. and Hahm T.S. 2006 *Plasma Phys. Control. Fusion* **48** A409
[18] Kwon J.M., Yi S., Rhee T., Diamond P.H., Miki K., Hahm T.S., Kim J.Y., Gürcan Ö.D. and McDevitt C. 2012 *Nucl. Fusion* **52** 013004
[19] Wang W.X., Hahm T.S., Lee W.W., Rewoldt G., Manickam J. and Tang W.M. 2007 *Phys. Plasmas* **14** 072306
[20] Yi S., Kwon J.M., Diamond P.H. and Hahm T.S. 2014 *Phys. Plasmas* **21** 092509
[21] Hahm T.S. and Burrell K.H. 1995 *Phys. Plasmas* **2** 1648
[22] Citrin J. *et al* 2013 *Phys. Rev. Lett.* **111** 155001
[23] Yi S., Kwon J.M., Diamond P.H. and Rhee T. 2012 *Phys. Plasmas* **19** 112506
[24] Inagaki S. *et al* 2014 *Nucl. Fusion* **54** 114014